Revista Mexicana de Astronomía y Astrofísica

Revista Mexicana de Astronomía y Astrofísica
Universidad Nacional Autónoma de México
rmaa@astroscu.unam.mx
ISSN (Versión impresa): 0185-1101
MÉXICO

2006
S. Medina / M. Peña / C. Morisset / G. Stasinska
GALACTIC PLANETARY NEBULAE WITH WOLF-RAYET NUCLEI III. KINEMATICAL ANALYSIS OF A LARGE SAMPLE OF NEBULAE
Revista Mexicana de Astronomía y Astrofísica, abril, año/vol. 42, número 001
Universidad Nacional Autónoma de México
Distrito Federal, México
pp. 53-74

Revista Mexicana de Astronomía y Astrofísica, **42**, 53–74 (2006)

GALACTIC PLANETARY NEBULAE WITH WOLF-RAYET NUCLEI III. KINEMATICAL ANALYSIS OF A LARGE SAMPLE OF NEBULAE[1]

S. Medina,[2] M. Peña,[2] C. Morisset,[2] and G. Stasińska[3]

Received 2005 August 8; accepted 2005 December 6

RESUMEN

Se midieron y analizaron las velocidades de expansión ($V_{\rm exp}$) de diferentes iones y el ancho en la base de las líneas en 24 nebulosas planetarias (NPs) con núcleo [WC] (WRPNe), 9 NPs ionizadas por WELS (WLPNe) y 14 NPs normales. El estudio comparativo del comportamiento cinemático de los objetos muestra que las WRPNe tienen $V_{\rm exp}$ 40–45% mayores y más turbulencia que las WLPNe y PNe normales. Las WLPNe tienen comportamiento cinemático muy similar a las NPs normales. Todos los objetos muestran $V_{\rm exp}$ que aumenta con los indicadores de edad (densidad nebular y temperatura de las estrellas), pero el efecto es mayor en las WRPNe evolucionadas, sugiriendo que el intenso viento estelar ha acelerado a la nebulosa por largo tiempo. En los objetos no-WR, la aceleración de la nebulosa se detiene cuando la estrella alcanza una temperatura del orden de 90,000 – 100,000 K y $V_{\rm exp}$ llega a un valor máximo de 30 km s^{-1}. Las WRPNe alcanzan $V_{\rm exp}$ máximas del orden de 40 km s^{-1}. Encontramos que $V_{\rm exp}(N^+)$ es ligeramente mayor que $V_{\rm exp}(O^{++})$ en todo tipo de objetos, indicando que las nebulosas muestran aceleración en las capas externas.

ABSTRACT

Expansion velocities ($V_{\rm exp}$) of different ions and line widths at the base of the lines are measured and analyzed for 24 PNe with [WC]-type nuclei (WRPNe), 9 PNe ionized by WELS (WLPNe) and 14 ordinary PNe. A comparative study of the kinematical behavior of the sample clearly demonstrates that WRPNe have on average 40–45% larger $V_{\rm exp}$, and possibly more turbulence than WLPNe and ordinary PNe. WLPNe have velocity fields very much like the ones of ordinary PNe, rather than the ones of WRPNe. All the samples (WRPNe, WLPNe and ordinary PNe) show expansion velocities increasing with age indicators, for example $<V_{\rm exp}>$ is larger for low-density nebulae and also it is larger for nebulae around high-temperature stars. This age effect is much stronger for evolved WRPNe, suggesting that the [WC] winds have been accelerating the nebulae for a long time, while for non-WRPNe the acceleration seems to stop at some point when the star reaches a temperature of about 90,000 – 100,000 K. Non-WR nebulae reach a maximum $V_{\rm exp} \leq 30$ km s^{-1} while evolved WRPNe reach maximum $V_{\rm exp}$ of about 40 km s^{-1}. For all kinds of objects (WRPNe and non-WRPNe) it is found that on average $V_{\rm exp}(N^+)$ is slightly larger than $V_{\rm exp}(O^{++})$, indicating that the nebulae present acceleration of the external shells.

Key Words: **PLANETARY NEBULAE: INDIVIDUAL: NGC 6369, M 1-32, BD+30°3639, K 2-16 — STARS: WOLF-RAYET**

[1]Based on data collected at the Observatorio Astronómico Nacional, San Pedro Mártir, B. C., México.

[2]Instituto de Astronomía, Universidad Nacional Autónoma de México, México.
[3]LUTH, Observatoire de Meudon, France.

1. INTRODUCTION

Among galactic planetary nebulae with known central stars, less than 15% have nuclei presenting Wolf-Rayet features. All these stars have been classified as belonging to the [WC] spectral type, showing almost pure helium and carbon in their atmospheres (e.g., Tylenda, Acker, & Stenholm 1993; Hamann 1997). The only possible [WN] central star in the Galaxy was reported by Morgan, Parker, & Cohen (2003).

Many recent studies have been devoted to these planetary nebulae (hereinafter WRPNe) and their central stars with interesting new results. Górny & Stasińska (1995) found that the physical properties and chemical abundances of WRPNe were not different from those of non-WRPNe, except for higher expansion velocities. Since then, Peña et al.(1998, Paper I) found that central stars of different initial masses can pass through the same [WC] stage and Peña, Stasińska, & Medina (2001, Paper II) reported an unexpected behavior of the [O III]/[N II] electron temperature ratios for WRPNe which does not seem to be present in non-WRPNe. In addition, Górny et al. (2001) have found that in an infrared diagram (H–K) versus (J–H), WRPNe spread over a larger zone than non-WRPNe which is probably more reflecting differences in dust and stellar properties rather than differences in nebular properties. Acker et al. (2002) have concluded that WRPNe show similar expansion velocities but larger turbulent velocities that normal PNe, and recently Gesicki, Acker, & Zijlstra (2003) concluded that the WRPNe tend to show strong acceleration at the ionization front and strong turbulent motions.

For the central stars, several scenarios to produce such H-deficient low-mass stars have been proposed (e.g., Blöcker 2001; Herwig 2001). In addition, Górny & Tylenda (2000) and De Marco (2002) have provided further arguments for the existence of the evolutionary sequence: [WC]-late → [WC]-early stars, ending with the PG 1159 type stars, proposed by Acker, Gorny, & Cuisinier (1996) and Hamann (1997). However, this proposition is still being debated (Hamann, Todt & Grafener 2005).

Parthasarathy, Acker, & Stenholm (1998) have claimed that "weak emission line stars" (WELS), as defined by Tylenda et al. (1993), are an intermediate stage between [WC] and PG 1159 stars. However, Peña et al. (2001) have argued that PNe around WELS are more similar to ordinary PNe than to WRPNe and consider doubtful the proposition of Parthasarathy et al.

Between 1995 and 2000, we have performed systematic observations of WRPNe, to gather a homogeneous high-resolution spectroscopic data set for studying the nature and evolutionary status of WRPNe. From these data, in Paper I we presented detailed photoionization models for a sample of very high excitation nebulae ionized by [WC 2-3] central stars, and in Paper II we reported line intensities, physical conditions and chemical composition for 34 PNe with nuclei of all [WC] spectral types, including a few WELS.

In this work, our high resolution data are employed to analyze the kinematical behaviour of 24 WRPNe (most of them presented in Paper II) with the purpose of studying the effects of the powerful [WC] winds on the nebular shells. We analyze some phenomena affecting the nebular profiles such as expansion velocities, turbulence and high velocity material. In particular we address the problem of whether WRPNe present higher expansion velocities and/or turbulence than non-WRPNe. To perform our analysis we have included a sample of 14 ordinary planetary nebulae (i.e., whose nuclei are neither WR nor WELS) which are useful as a control sample to confirm that any special trend found for WRPNe is not an instrumental effect. Nine PNe ionized by a WELS (hereinafter WLPNe) have been included also in the analysis.

In § 2, the observations and data reduction are described. The line profiles are discussed in § 3. The expansion velocities derived for the sample are presented and analyzed in § 4, where a brief discussion regarding turbulence can be found. In § 5, we present the line widths at the base of lines, searching for the highest velocity material. The kinematical analysis of selected nebular lines is presented in § 6. Our main conclusions are summarized in § 7. Finally, two Appendices have been included, where we present some examples of our data and discuss some objects with particularly interesting profiles or kinematics.

2. OBSERVATIONS AND DATA REDUCTION

High-resolution spectroscopic data were systematically gathered with the 2.1 m telescope (f/7.5) at the Observatorio Astronómico Nacional, San Pedro Mártir, B. C., México on 1995 July 29–31, 1996 June 14–17, 1997 August 3–4, 1998, December 11–14, 1999 October 4–7, and 2000 November 1–3. The REOSC Echelle Spectrograph plus the University College London camera (described by Levine & Chakrabarty 1993) were always used. Two different CCD detectors were employed: for observations in 1995 and 1996 we used a CCD Tektronix

TABLE 1

OBSERVING LOG[a]

PN G	Usual name	Obs. dates (dd/mm/yy)
013.7 − 10.6	YC 2-32	02/11/00
037.7 − 34.5	NGC 7009	01/11/00
084.9 − 03.4	NGC 7027	02/11/00
103.7 + 00.4	M 2-52	02/11/00
104.4 − 01.6	M 2-53	01-02/11/00
118.0 − 08.6	Vy 1-1	02/11/00
130.3 − 11.7	M 1-1	01-02/11/00
133.1 − 08.6	M 1-2	01-02/11/00
147.4 − 02.3	M 1-4	03/11/00
159.0 − 15.1	IC 351	11/12/98
166.1 + 10.4	IC 2149	13/12/98
194.2 + 02.5	J 900	02/11/00
196.6 − 10.9	NGC 2022	02/11/00
215.2 − 24.2	IC 418	12-13/12/98
221.3 − 12.3	IC 2165	03/11/00
243.8 − 37.1	PRTM 1	12-13-14/12/98
294.1 + 43.6	NGC 4361	04/10/99

[a]Observing set-up: 2048×2048 ($14\times14\,\mu m^2$) pixel CCD detector; slit dimensions: $4''\times13''$, oriented E–W; wavelength range 3360–7360 Å, spectral resolution ~ 0.2 Å. Extraction window: $4''\times3''$, for all the objects.

of 1024×1024 (23μm) pixels, providing an average spectral resolution of 0.3 Å (about 18 km s^{-1} in velocity) with a 150μm slit width, and since 1997 we used a CCD Thomson of 2048×2048 (14μm) pixels, giving a resolution of 0.2 Å (about 11 km s^{-1}) with the same slit width.

The observations for most of WRPNe and WLPNe presented here were described in Paper II, where a detailed list of objects, observing dates, exposure times and instrumental set-up were given. In Table 1 we present the log of observations for objects not reported in Paper II (mainly WLPNe and ordinary PNe). As usual we have taken at least two consecutive observations for each object in each run. Different exposure times (from 2 to 15 minutes) were used to obtain a S/N better than 3 for the weak lines without saturating the most intense ones. The different exposures for the same object were averaged to increase the S/N. The slit was always E–W oriented. In this work, the reported data correspond always to those obtained for the central zone (the slit was centered on the central star). For all the objects we covered a wide spectral range (at least from 3700 to 6800 Å); therefore lines for high and low ionized species were obtained. This is important for studying the kinematics on different zones of the nebula where such species reside.

A Th–Ar lamp was used for wavelength calibration in all the spectral ranges and a tungsten bulb was used for flat fielding. Standard stars from the list by Hamuy et al. (1992) were observed each night for flux calibration. Data reduction was performed using the package IRAF[4] and includes standard bias-subtraction and flat-field correction for all spectra.

In Table 2, we present some nebular characteristics (diameter, electron temperatures from the [O III] lines, densities from the [S II] lines and ionic abundance ratios) for all the objects for which the kinematical analysis is performed. Most of the data was taken from Papers I and II. For the new objects (Table 1) the nebular characteristics were derived by using the same procedures as reported in those papers. In addition, in columns 8 to 11 of Table 2 we present the stellar classification, stellar temperature and wind parameters, taken from the literature. All these data will be used in the interpretation of the kinematical data.

3. LINE PROFILES

[WC] stars present intense and wide emission lines of helium, carbon, and other elements, whose wavelengths occasionally coincide with the wavelengths of some nebular lines. For instance, this is the case of the nebular He II, He I, and H Balmer lines which coincide with stellar He II and He I lines, and especially this is the case of [N II] λ6583 and [S II] λ6731 which appear on the top of some C II multiplet 2 lines. High spectral resolution is necessary to safely deblend the nebular and stellar components and to study the nebular profiles. This is important for all [WC]-type objects but it is essential for compact nebulae around [WC]-late stars where the stellar winds show terminal velocities of a few 100 km s^{-1}(see Table 2), and the stellar lines present a FWHM of a few Å. Therefore a spectral resolution better than 5000 is necessary. This is one of the advantages of our spectra (resolution of 18,000). In Appendix A, we present stellar and nebular lines for some of our objects (particularly [WC]-late type objects) to show that our spectral resolution allows us to safely deblend both components for most of the objects. Thus the nebular lines have been measured without stellar contamination.

[4]IRAF is distributed by NOAO, which is operated by AURA, Inc. under contract with the NSF.

Also, the high spectral resolution of our data allows us to obtain well resolved nebular profiles for all the sample, except for a couple of objects showing FWHM of lines smaller than our instrumental resolution. Therefore, we have an extensive data set including different kind of objects, obtained in a consistent way, which allows us to perform a reliable comparative analysis of the kinematics. First we will analyze the adequacy of deriving expansion velocities from the line profiles.

3.1. *Line Profiles and Velocity Field*

A nebular line profile depends on several internal properties such as the nebular morphology, the density distribution, the thermal and ionization structures, the turbulence, the expansion velocity, etc. In addition, the observed profile also depends upon the spectral resolution and the position and dimensions of the slit: for instance, when the nebula is extended and the slit just covers the central zone, the classical double-peak profile is obtained. Many authors have derived the nebular expansion velocity, $V_{\rm exp}$, as half the separation of the peaks. On the other hand, when the slit includes the entire nebula, or when we are dealing with a filled nebula (with a very small inner hole, as could be the case of a very young nebula) a single profile is usually observed. In such a case, the half width at half maximum (HWHM) has been used to measure $V_{\rm exp}$. In our sample, many nebulae do not present a well defined shell, or they have knots at different velocities, showing then complex profiles, for which is difficult to derive $V_{\rm exp}$ in a straightforward manner.

An ad-hoc detailed kinematical model, including the density distribution (3D-morphology) and the ionization and thermal structuctures of the nebula, would be required to deconvolve the effect of each contribution to the line profile. An approach to this procedure, using a spherically symmetric model, can be found in Gesicki, Acker, & Szczerba (1996), Gesicki, Acker, & Zijlstra (2003), and other papers by the same authors. More recently, tomography techniques or 3D spatio-kinematic models have been used to calculate the line profiles of some individual nebulae (Sabbadin et al.2004 and references therein; Monteiro et al. 2005). The main weaknesses of such a procedure are that the results are strongly model dependent, the derived model is probably not unique, and it is very time consuming.

It is beyond the scope of this work to develop such a model for each of our objects. Our main aim is to derive reliable expansion velocities for different ions (which, due to the ionization structure, are located at different distances from the central star) to compare the behavior of WRPNe with those of non-WRPNe and to address, if possible, the effects due to turbulence.

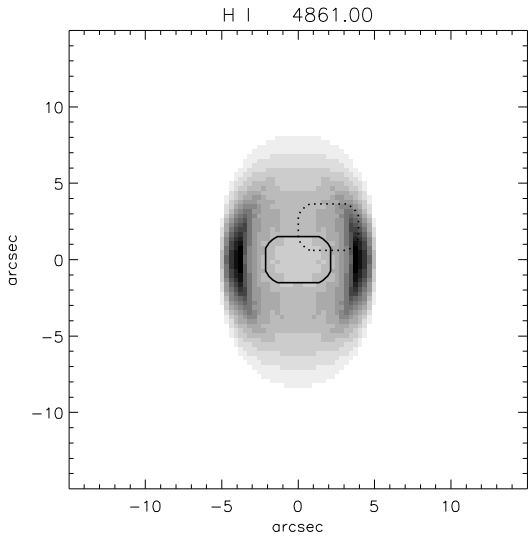

Fig. 1. The Hβ surface brightness of the modeled nebula is shown. Two slits of $3'' \times 4''$ centered and off-center are superimposed. They are used to produce "observed profiles" (see § 3.1).

To relate the line profiles with the values of the real expansion velocities for our objects in a consistent manner, we have used the code NEBU-3D, presented by Morisset, Stasińska, & Peña (2005), to compute a spatio-kinematic model for analyzing the line profile behavior of a simple and common case: an ellipsoidal nebula ionized by a central star with an effective temperature of 80,000 K and a luminosity of 10^{35} erg s^{-1}. The chemical abundances are solar. The nebula has an internal elliptical hole with the major axis twice the minor axis. The orientation of the polar axis makes an angle of 45° with the line of sight (thus the nebula is in between "polar-on" and "face on" orientations). The density is constant in the radial direction, but varying with the polar angle according to $\mathrm{N(H)_{inner}} = \mathrm{N(H_0)} \times (R_0/R_{inner})^2$, where $\mathrm{N(H_0)}$ and R_0 are the hydrogen density and the inner radius at the equator. The dependence of N(H) with the polar angle is included in the parameter R_{inner} which follows the ellipsoidal form.

Figure 1 presents the Hβ surface flux distribution, projected on the sky. The nebular dimensions projected on the sky are about $5'' \times 7''$ (a distance of 1.87 kpc is assumed). Two "observing slits" (a $3'' \times 4''$ slit, centered, and a similar one, off-center) have been superposed. These slits are used to extract "observational" data to compare with our own.

TABLE 2

NEBULAR AND STELLAR PHYSICAL PARAMETERS[a]

PN G	Name	T_e (10^4 K)	N_e (cm^{-3})	He^{++}/He^+	O^{++}/O^+	ϕ (arcsec)	[WC][b]	T_* (10^3 K)	v_∞ (km s^{-1})	log $\dot{M}$ ($M_\odot$ yr^{-1})	Ref.
001.5 − 06.7	SwSt 1	1.06	30000	0.0	0.3	5	9	40	900	−6.72	dM01
002.4 + 05.8	NGC 6369	1.01	3220	0.1	15.7	38	4	150	1200	−6.15	KH97a
002.2 − 09.4	Cn 1-5	1.09	4700	0.0	82.8	7	4	< 57	···	···	TS94
003.1 + 02.9	Hb 4	0.96	4600	0.1	33.9	7.2	3−4	86	···	···	TS94
004.9 + 04.9	M 1-25	0.80	10400	0.0	43.6	3.2	6	60	···	···	L96
006.8 + 04.1	M 3-15	0.87	7443	0.0	38.8	4.5	5	55	···	···	ZK93
011.9 + 04.2	M 1-32	0.99	6720	0.0	12.1	9	4−5	66	···	···	TS94
012.2 + 04.9	PM 1-188	0.94	200	0.0	0.03	4	10	35	360	−5.70	LH98
017.9 − 04.8	M 3-30	1.03	525	0.9	27.2	20	2	97	···	···	TS94
027.6 + 04.2	M 2-43	1.05	10100	0.0	14.3	1.5	8	65	850	−6.08	LH98
029.2 − 05.9	NGC 6751	1.12	2730	0.0	5.2	20.5	4	135	1600	−6.12	KH97b
048.7 + 01.9	He 2-429	0.77	6810	0.0	3.6	4.2	4−5	···	···	···	
061.4 − 09.5	NGC 6905	1.21	1530	2.9	58.6	40	2−3	141	1800	−6.32	KH97a
064.7 + 05.0	BD+30°3639	1.01	21200	0.0	0.0	7.7	9	47	700	−4.87	L96
068.3 − 02.7	He 2-459	2.00:	17400	0.0	···	1.3	8	77	1000	−5.01	L97
089.0 + 00.3	NGC 7026	0.92	3250	0.2	14.7	20	3	130	3500	−6.34	KH97a
096.3 + 02.3	K 3-61	0.89	1690	0.0	···	6.1	4−5	···	···	···	
120.0 + 09.8	NGC 40	1.00	1980	0.0	0.1	48	8	78	1000	−5.62	L96
130.2 + 01.3	IC 1747	1.12	2380	0.2	78.6	13	4	126	1800	−6.58	KH97a
144.5 + 06.5	NGC 1501	1.05	1020	0.7	···	52	4	135	1800	−6.28	KH97a
146.7 + 07.6	M 4-18	0.86	6350	···	0.0	3.7	10	31	160	−6.05	dMC99
161.2 − 14.8	IC 2003	1.28	3840	1.38	21.4	8.6	3	88	···	···	TS94
243.3 − 01.0	NGC 2452	1.30	1590	0.7	6.0	19	2	141	3000	−6.20	KH97a
352.9 + 11.4	K 2-16	1.17	504	···	0.4	13.5	11	30	300	−6.36	L97b
009.4 − 05.0	NGC 6629	0.84	3470	0.0	13.5	15.5	wl	< 52	···	···	TS94
010.8 − 01.8	NGC 6578	0.79	2270	0.0	240	8.5	wl	65	···	···	TS94
011.7 − 00.6	NGC 6567	0.95	4360	0.01	28.3	7.6	wl	61	1950	···	TS94
096.4 + 29.9	NGC 6543	0.79	5640	0.0	75.4	19.5	wl	< 66	1900	−7.4	TS94
100.6 − 05.4	IC 5217	1.12	8850	0.1	93.9	6.6	wl	72	···	···	TS94
159.0 − 15.1	IC 351	1.31	2500	1.0	24.7	7	wl	85	···	···	TS94
194.2 + 02.5	J 900	1.13	1110	0.7	9.2	9	wl	123	···	···	TS94
221.3 − 12.3	IC 2165	1.41	3984	0.8	19.0	9	wl	153	···	···	TS94
356.2 − 04.4	Cn 2-1	0.97	5320	0.07	74.2	2.4	wl	84	···	···	P-M91
013.7 − 10.6	YC 2-32	0.88	3337	0.03	···	15	pn	68	···	···	TS94
037.7 − 34.5	NGC 7009	1.08	4371	0.3	151.8	28.5	pn	85	2750	−8.55	TS94
084.9 − 03.4	NGC 7027	1.64	30000	1.1	2.8	14	pn	175	···	···	TS94
103.7 + 00.4	M 2-52	1.41	879	1.3	127.1	14	pn	···	···	···	
104.4 − 01.6	M 2-53	1.11	496	0.1	1.6	14.8	pn	112	···	···	TS94
118.0 − 08.6	Vy 1-1	0.99	2101	0.0	56.6	5.2	pn	32	···	···	TS94
130.3 − 11.7	M 1-1	2.7:	3000	46.7	7.2	6	pn	87	···	···	TS94
133.1 − 08.6	M 1-2	···	4264	0.02	···	18	pn	51	···	···	TS94
147.4 − 02.3	M 1-4	1.03	6276	0.06	···	4	pn	67	···	···	TS94
166.1 + 10.4	IC 2149	0.95	10000	0.0	6.8	8.5	pn	< 49	1290	−7.7	TS94
196.6 − 10.9	NGC 2022	1.51	800	8.7	62.5	19	pn	114	···	···	TS94
215.2 − 24.2	IC 418	0.87	18000	> 0.1	0.44	12	pn	53	1050	−8.2	TS94
243.8 − 37.1	PRTM 1	1.63	1200	7.8	> 300	23	pn	90	···	···	P90
294.1 + 43.6	NGC 4361	1.93	800	> 19	> 180	63	pn	95	···	···	TS94

[a]Nebular data are mostly from Paper II. Nebular diameter ϕ is from Acker et al. 1992. T_*, v_∞ and log $\dot{M}$ values were taken from literature, and the references are: dM01: De Marco et al. (2001); dMC99: De Marco & Crowther (1999); KH97a: Koesterke & Hamann (1997a); KH97b: Koesterke & Hamann (1997b); L96: Leuenhagen et al. (1996); L97a: Leuenhagen (1997a), L97b: Leuenhagen (1997b); LH98: Leuenhagen & Hamann (1998); P90: Peña et al. (1990); P-M91: Preite-Martinez et al. (1991); TS94: Tylenda & Stasińska (1994); ZK93: Zhang & Kwok (1993).

[b]Central star type is as following: a number indicates the [WC] spectral type, *wl* is for WELS and *pn* for normal stars.

The expansion velocity of the modeled nebula grows with the distance from the star as V = 60 R/R_{max} km s^{-1} (R_{max} = 4.2 10^{17} cm is the distance from the central star to the pole). A turbulent component of 0.5 km s^{-1} has been added to the expansion.

We consider that this hypothetical nebula represents adequately the majority of nebulae. We have verified that for other morphologies (like spherical or bipolar nebulae) the results do not differ significantly from the conclusions presented here. A very simple spherical case has been analyzed by Gesicki & Zijlstra (2000) providing very similar results. An extensive sample of elliptical and bipolar objects seen in different orientations and with different conditions will be presented in a catalog of profiles to be published elsewhere (Morisset et al., in preparation).

The main characteristics of our modeled nebula are presented in Figure 2. The upper panels show the density, temperature and velocity structures as function of the distance from the central star (in units of R_{max}) along the equator (solid lines) and along the polar axis (dotted lines). The second row of panels presents the surface brightnesses computed for Hβ, He II λ4686, and [N II] λ6583, as a function of the distance from the central star along the same directions. The third row of panels presents the line profiles of Hβ, He II λ4686, and [N II] λ6583 as a function of the velocity, obtained by integrating through the two slits shown in Fig. 1. The solid lines present the profiles through the centered slit (this slit has the same size and position as our extraction window), while the dotted lines show the profile through the off-center slit. The lowest row of panels shows the profiles through a $30'' \times 30''$ slit which includes the whole nebula. Superposed to these profiles we have traced horizontal lines indicating the values of $V_{\rm exp}$ as measured with different methods: the heavy solid line is the "real velocity", computed as the average velocity of the ion weighted by the emissivity of the line, the thin solid line is the peak-to-peak velocity, the dotted line is the HWHM velocity and the dashed line is the velocity at 1/10 the maximum intensity of the profile (V_{10}, see § 5).

The main results of our model, as it is observed in Fig. 2, show that when the nebula is well centered in the slit and it is fully resolved (third row of panels) it presents symmetric double-peak profiles and that half the peak-to peak separation is a very good approach for the "real velocity", underestimating it by less than 10%.

The HWHM of the profile overestimates the "real velocity" by about 10%. The profiles obtained when the slit is off-center (dotted profiles) are always asymmetrical and it is very difficult to measure the expansion velocities from them, as the separation between peaks is smaller than the centered case.

When the nebula is fully included in the slit, it presents single Gaussian profiles and the HWHM of the profiles is a good measurement of the expansion velocity within 20%. As expected due to the adopted velocity law, [N II] λ6583 presents a higher expansion velocity than He II λ4686, and Hβ, and the latter one shows much wider lines due to the thermal broadening (which is included).

V_{10} is always larger than the 'real velocity' by about 30–40%, but it is closer to the velocity of the most external (although faint) zones and it is useful to detect high-velocity low-emission components in the gas.

3.2. *Our Observed Profiles*

The line profiles obtained for our objects fall mainly into five different categories: (a) symmetric double-peak profiles found mainly in extended objects, (b) single Gaussian-type profiles usually found for compact symmetrical nebulae, the prototype being M 4-18 whose [N II]λ6583 profile is shown in Figure 3a, (c) single asymmetrical profiles as seen in Fig. 3b, usually produced by asymmetric nebulae (or produced by aspherical nebulae where the slit did not cross exactly the center), (d) single profiles with wide wings or 'shoulders' as shown in Fig. 3c (this could be due to high velocity gas or highly turbulent gas; high velocity components have been reported for some objects, e.g., De Marco, Barlow, & Storey 1997), (e) complex profiles showing several components which usually correspond to knotty nebulae as the one presented in Fig. 3d.

For the first two categories, $V_{\rm exp}$ can be measured safely in the classical form: from half the peak-to-peak separation for the well-resolved objects and from the HWHM for objects showing single lines with no asymmetries nor complex profiles. Our measurements are presented in the next section. Objects with very asymmetrical profiles, for which it is very difficult to define the expansion velocity in a simple way, were excluded from the $V_{\rm exp}$ analysis. For all the objects, the type of line profile is indicated in the last column of Table 5.

For the kinematical analysis, the profiles of Hβ, He II λ4686, [O III] λ5007, and [N II] λ6583 lines were measured when available. The purpose for selecting these lines was to study possible kinematical differences between lines arising from ions located at different distances from the central star. For instance, while the Hβ line is mapping the whole nebula, He II λ4686 and [O III] λ5007 lines give information about the inner and intermediate regions, and [N II] λ6583 gives information about the outer regions.

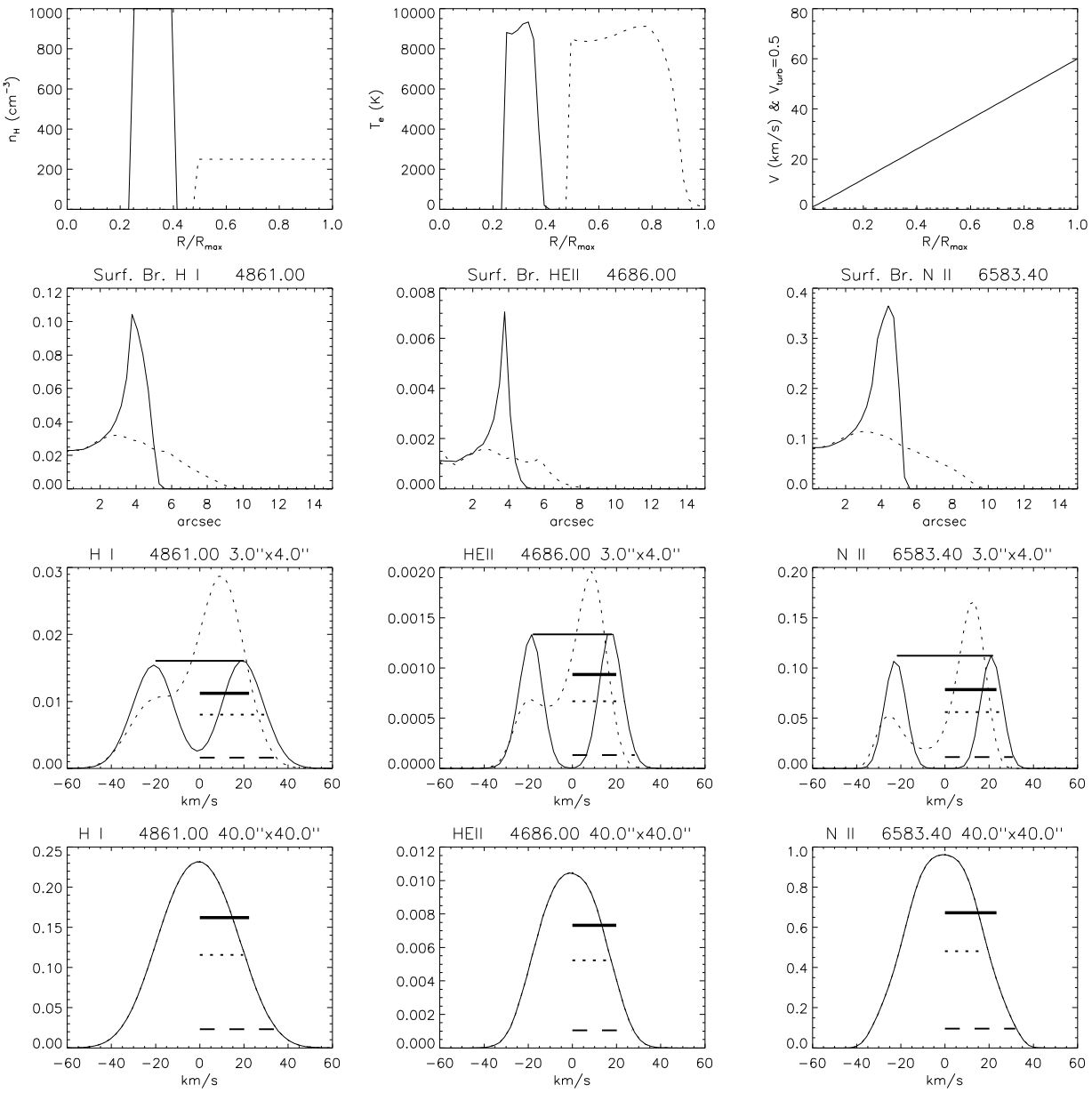

Fig. 2. Upper panels show the density, temperature and velocity distributions in the modeled nebula. The second row of panels shows the surface brightness along the equator (solid lines) and the polar axis (dotted lines) for several emission lines. The third row of panels shows the line profiles obtained through the centered slit (solid lines) and the off-center slit (dotted profile). The horizontal lines represent the "real velocity" (heavy solid line), the peak-to-peak (thin solid line), the HWHM (dotted line) and V_{10} (dashed line) velocities, for the centered slit. The lowest panels show the line profiles through a slit of $30'' \times 30''$, including the whole nebula.

4. EXPANSION VELOCITIES

4.1. *Objects with Split Profiles*

Twelve objects of our sample (six WRPNe, two WLPNe, and four ordinary PNe) present symmetrical split profiles. Remember that according to our model such profiles are observed for well resolved nebulae and half the peak-to-peak separation is a good approach for $V_{\rm exp}$. Values for [O III] λ5007, Hβ, [N II] λ6583, and He II λ4686 lines are presented in Table 3. Typical errors are ± 5 km s^{-1}. The [WC]

type of the central stars or an indication if the star is a WELS or a "normal" central star is listed in Col. 3.

The line widths (FWHM) for each component of Hβ, ΔV_1, and ΔV_2 (in km s^{-1}), are also listed. The instrumental and thermal widths have been subtracted from each line width by assuming that they add in quadrature. The instrumental widths were measured from the comparison lamp lines (using the same slit widths as in the observations) and they turned out to be 18 km s^{-1} for observations prior to 1997 (23μ pixel size CCD) and 12 km s^{-1} for those since 1997 (14μ pixel size CCD). The thermal contribution to line width for any ion can be expressed as $\Delta V_{\rm th} = 21.4\sqrt{t_{\rm e}/A}$ (km s^{-1}), where $t_{\rm e}$ is the electron temperature in units of 10^4 K and A is the atomic mass (Lang 1980); therefore for Hβ, $\Delta V_{\rm th} = 21.4\sqrt{t_{\rm e}}$ while for [O III], $\Delta V_{\rm th} = 5.35\sqrt{t_{\rm e}}$, etc. The electron temperature employed for each object has been listed in Table 2.

The individual line widths in Table 3, in the range of 18–30 km s^{-1}, are therefore mainly due to turbulence and possible velocity gradients within the shell. In this sense notice that the model presented in § 3, which has a velocity gradient producing $\Delta V \geq 20$ km s^{-1} from side to side of the shell, predicts a FWHM of about 5–6 km s^{-1}for the double-peak profiles (third row of panels in Fig. 2), after subtracting the thermal width. Our objects in Table 3 present much higher ΔV, possibly produced by turbulence.

Table 3 (see also § 6.1) shows that, for a given object, the expansion velocities from different ions are, in general, very similar, although most of the objects have slightly larger $V_{\rm exp}$([N II]) than $V_{\rm exp}$([O III]) or $V_{\rm exp}$(Hβ) which, as in our model, might be indicating that the expansion velocity increases with the distance from the central star. This fact, predicted by hydrodynamical models as due to acceleration of the external nebular material, was already noticed by Wilson (1950) for his sample of PNe.

Our $V_{\rm exp}$ values are equal, within uncertainties, to those from the catalogue by Weinberger (1989), which have been included in Col. 10 of Table 3. In Col. 11 we have also included the expansion velocities found by Acker et al. (2002), based upon modeling the velocity field, for the few objects in common; their $V_{\rm exp}$ values and ours coincide, except for the faint and extended WRPN K 2-16 for which Acker et al. give two different values. A deeper analysis of K 2-16 is found in the Appendix B.5.

For the sample presented in Table 3, we found that WRPNe have $V_{\rm exp}$ values (as measured from [O III] lines) ranging from 24 to 44 km s^{-1} with an average of 36 km s^{-1}, while WLPNe and ordinary PNe show $V_{\rm exp}$ from 17 to 26 km s^{-1} with an average of 21.5 km s^{-1}. That is $<V_{\rm exp}$(WRPNe)$>$ is 67% larger than $<V_{\rm exp}$(non-WRPNe)$>$. Therefore, definitely, WRPNe in this sample have larger expansion velocities than non-WRPNe (WLPNe and ordinary PNe). Also, a systematic trend of higher $V_{\rm exp}$ with earlier [WC] type seems to be present. This result will be strengthened in the following sections.

In addition to higher $V_{\rm exp}$, WRPNe seem also to show larger line widths than non-WR objects. This is particularly true for WRPNe with early [WC] stars such as NGC 6905, NGC 6369, NGC 6751, and NGC 1501, which in principle are more evolved, probably indicating large turbulence in these nebulae.

In conclusion, WRPNe with split profiles are showing higher expansion velocities and probably more turbulence than WLPNe and ordinary PNe. This does not agree with the results presented by Acker et al. (2002), who have concluded that the expansion velocities in WRPNe and non-WRPNe are similar but WRPNe are much more turbulent than non-WRPNe. In addition, their models would indicate that ordinary PNe present acceleration in the outer nebular zones, while WRPNe do not, which is not the case for our objects.

4.2. *Objects with Single Profiles*

The FWHM of [O III] λ5007, Hβ, [N II] λ6583, and He II λ4686 were measured for all the objects showing single symmetrical profiles (alternatively [N II] λ6548 was measured when the stellar C II lines were severely blended with [N II]λ6583. See Appendix A). Instrumental and thermal widths were subtracted as indicated in § 4.1. We have assumed that HWHM represents the expansion velocity plus turbulence. The results are presented in Table 4 where, in Col. 8, we have included $V_{\rm exp}$([O III]) from the compilation by Weinberger (1989) or from more recent literature, and in Col. 9, the values reported by Acker et al.(2002).

Although in this case it is more difficult to compare kinematical data measured by different authors using different procedures, it is found that the majority of our values coincides within a factor of 1.2 with those from the literature. For several objects (M 1-32, He 2-459, K 1-61, and YC 2-32), $V_{\rm exp}$ are determined for the first time.

Typical errors for our measurements are $\pm$6–8 km s^{-1} for [N II] and He II lines and $\pm$4 km s^{-1} for [O III] and Hβ lines. We have searched for systematic

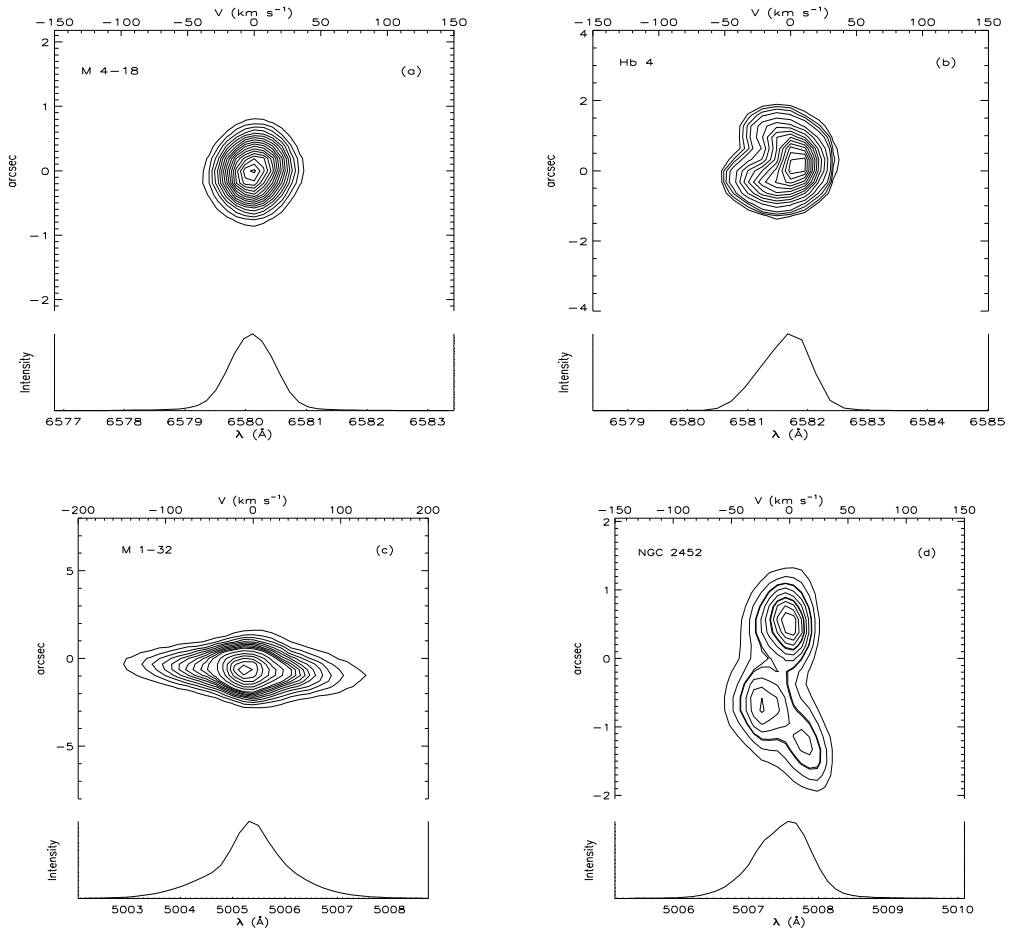

Fig. 3. Position-velocity diagrams and integrated profiles from the extracted spectra are shown featuring the different types of line profiles found in our sample. The different types are: (a) simple Gaussian [N II] λ6583 profile of M 4-18, (b) asymmetrical [N II] λ6583 profile of Hb 4, (c) [O III] λ5007 high velocity wings found in M 1-32, (d) knotty structure and complex [O III] λ5007 profile in NGC 2452. At the top of each figure, a velocity scale helps to visualize the velocity profile. The 0 corresponds to the maximum line intensity.

errors (as, e.g., a dependence of $V_{\rm exp}$ as a function of electron temperatures) and found that these errors appear to be negligible. Also, possible contamination of nebular lines with stellar emission lines, producing artificial broadening of nebular lines, is discarded as a source of important systematic errors (see Appendix A). Systematic trends of $V_{\rm exp}$ with electron density and stellar temperature are found for all the sample but these are real trends and they are discussed in the following sections.

$V_{\rm exp}$ averages of the 14 WRPNe in Table 4 are 23, 23, and 25 km s^{-1}, for [O III], Hβ and [N II], respectively. The corresponding averages for the 5 WLPNe are 19, 18, and 22 and for the ordinary PNe they are: 19, 17, and 20. WLPNe and ordinary PNe show a very similar behavior and can be put together in a single sample, non-WRPNe, showing averages of 19, 18, and 20 km s^{-1} for [O III], Hβ, and [N II]. Therefore, the averages for WRPNe are 20–25% larger than the corresponding averages for non-WRPNe indicating that WRPNe have wider lines. In this case we cannot disentangle expansion velocities from turbulence, but this result is consistent with the results found in § 4.1 of higher expansion velocities and probably higher turbulence in WRPNe than in non-WRPNe.

As in the case of double-peak objects, here the $V_{\rm exp}$ average for [N II] is about 2 km s^{-1} larger than the corresponding values for [O III], regardless of whether they are WRPNe or non-WRPNe, confirming that the external shells might be expanding faster in all kinds of nebulae.

TABLE 3

EXPANSION VELOCITIES AND TURBULENCE FOR NEBULAE WITH DOUBLE PEAK LINES

PN G	Name	[WC][a]	$V_{\rm exp}$ (km s^{-1})[b]				ΔV_1[b]	ΔV_2[b]	$V_{\rm exp}$(OIII)[c]	$V_{\rm exp}$[c]
			[O III]	Hβ	[N II]	He II	Hβ	Hβ	W89	A02
061.4 − 09.5	NGC 6905	2-3	44	41	46	40	25	17	44	···
002.4 + 05.8	NGC 6369	4	36	36	37	38	24	38	42	···
029.2 − 05.9	NGC 6751	4	42	40	40	···	24	29	40	41
144.5 + 06.5	NGC 1501	4	40	40	42	38	20	19	37	40
120.0 + 09.8	NGC 40	8	30	26	26	···	18	< 15	29	···
352.9 + 11.4	K 2-16	11	24	24	26	···	22	16	···	34 or 38
100.6 − 05.4	IC 5217	wl	18	18	23	18	16	20	23	···
011.7 − 00.6	NGC 6567	wl	17	18	27	···	< 20	< 20	19	···
037.7 − 34.5	NGC 7009	pn	20	18	21	16	< 15	< 15	21	···
196.6 − 10.9	NGC 2022	pn	24	21	21	23	16	20	27	···
243.8 − 37.1	PRTM 1	pn	24	23	···	23	28	26	···	···
294.1 + 43.6	NGC 4361	pn	26	22	···	22	32	20	21	···

[a]Central star type as in Table 2.

[b]Uncertainties: ± 5 km s^{-1} for $V_{\rm exp}$, and ± 8 km s^{-1} for line widths. ΔVs were corrected for thermal and instrumental widths.

[c]References are: W89: Weinberger (1989); A02: Acker et al. (2002).

5. LINE WIDTHS AT THE BASE OF LINES

Considering that an important fraction of PNe shows kinematical features like ansae, BRETS, FLIERS, jets, high velocity ejecta, etc., (see Balick & Adam 2002 for a complete list and definition of these terms), all of them produced by non-spherical, bipolar, multipolar or asymmetrical ejections of the central star, it seems likely to expect some additional perturbations in the velocity field of WRPNe as compared with non-WRPNe, caused by the high mass-loss [WC] wind. For instance, the hydrodynamical computations of García-Segura & McLow (1995) have shown that the expansion of a hot bubble pushed by a WR wind results in a filamentary broken shell with probably large turbulence.

Therefore, in order to perform a comparative kinematical analysis of all our sample, including all these effects, we have decided to consider the nebular gas showing the highest velocity relative to the central star. This can only be measured at the base of the line profiles (half the full width at zero intensity). To avoid any noise disturbance due to the low signal at the base of the lines, we measured such a velocity as half the width of the line profile at one tenth maximum intensity (V_{10}), after subtracting the instrumental and thermal widths as described in § 3.1. A similar treatment was previously used by Dopita et al. (1985) to determine expansion velocities of a sample of planetary nebulae in the SMC.

To carry out a systematic treatment of all the observed data, V_{10} was determined for all the objects, including those cases where a single Gaussian adequately reproduced the shape of the lines or when the line profile showed a double peak (objects in Tables 3 and 4). In the latter case, half the full width at 1/10 intensity of each component was added to the peak-to-peak separation. It can be easily calculated that, for a single Gaussian profile, half the full width at 1/10 I max can be expressed as:

$$V_{10} = 0.911 \text{ FWHM} \quad (\text{km s}^{-1}) ;$$

while for double peak profiles (two Gaussians), it is found that:

$$V_{10} = V_{\rm exp} + 0.455\,(\Delta V_1 + \Delta V_2) \quad (\text{km s}^{-1}) .$$

We have used these expressions to derive V_{10} for our objects in Tables 3 and 4. For non-Gaussian, wing-extended, or complex profiles, V_{10} was measured directly from the line profiles.

V_{10} derived in such a way includes not only the expansion velocity of the shell, but also the turbulence of the gas and faint high velocity components,